Chemical Engineering Science 316 (2025) 121896

Contents lists available at ScienceDirect

Chemical Engineering Science

journal homepage: www.elsevier.com/locate/ces

A CFD-based approach to study cavitation in high-pressure homogenizer valves. Part 2. Cavitation intensity

Andreas Håkansson [a,*], Eva Rütten [b], Vivek V. Ranade [c]

[a] Department of Process and Life Science Engineering, Lund University, Lund, Sweden
[b] Institute of Process Engineering in Life Sciences, Food Process Engineering, Karlsruhe Institute of Technology, Karlsruhe, Germany
[c] Bernal Institute, University of Limerick, Ireland

ARTICLE INFO

Keywords:
Cavitation
High-pressure homogenization
CFD
Rayleight-Plesset model
Cavity implosion

ABSTRACT

Hydrodynamic cavitation take place in high-pressure homogenizer (HPH) valves. Cavitation wear, free radical formation and ultrasonic emissions are linked to the cavitation intensity. Cavitation intensity is also a key factor to understand any effect cavitation might have on particle breakup. Based on an approach used in previous studies on other devices, this contribution applies and tests a modelling framework for predicting and understanding cavitation intensity in a HPH valve. Effects of homogenizing pressure and backpressure are studied. Results show an increase in cavitation intensity with homogenizing pressure. The cavitation implosion induced dissipation rate of energy in a HPH is substantially lower than the dissipation rate of turbulent kinetic energy, which helps to explain previously reported empirical findings showing that cavitation does not break emulsion drops in HPHs. This contribution shows the importance of distinguishing between extent and intensity when discussing cavitation in HPH valves.

1. Introduction

As discussed in the introduction to the first part in this series (Rütten and Håkansson, 2025), hydrodynamic cavitation takes place in high-pressure homogenizer (HPH) valves under industrially relevant conditions. From an optimization perspective, it is important to understand this phenomenon, not at least in view of that cavitation gives rise to erosion wear (which is a major contribution to operating costs of homogenization) (Innings et al., 2011), and that extensive cavitation has been observed to suppress or delay emulsion drop breakup in devices designed to resemble HPH valves (Gothsch et al., 2015; Preiss et al., 2021).

The first part of this series utilized a CFD method to predict how the macroscopic flow is influenced by cavitation, where and how much vapour accumulates in the valve, and at what operating conditions this occur. These parameters describe the 'extent' of cavitation. However, many of the questions that arise from an applied perspective (intending to optimize design and operation) relate to cavitation 'intensity' rather than extent.

Here, 'intensity', should be understood as a measure of how forcefully the cavitation interacts with the surrounding fluids, particles, and solid walls, and how the cavitation causes desired or undesired transformations (e.g., Dastane et al., 2019; Gogate et al., 2001; Pandit et al., 2021; Pawar et al., 2017); see also discussion in Wu et al. (2020).

The previously reported experimental measures of cavitation in HPH valves (Floury et al., 2004; Gogate et al., 2001; Håkansson et al., 2010; Håkansson, 2025; Innings et al., 2011; Kurzhals, 1977; Lander et al., 2000; Schlender et al., 2015; Shirgaonkar et al., 1998) are controlled by cavitation intensity rather than by cavitation extent. For example, cavitation wear is typically understood from implosion of shockwaves or impingement of microjets on solid surfaces, or the acceleration of particles by microjets onto these solid surfaces (Gao et al., 2024; Sreedhar et al., 2017). Thus, to understand cavitation wear, it is more important to study the forcefulness of shockwaves, and velocities of microjets than the size of the vapour filled regions (Li et al., 2024; Yang et al., 2025).

Other examples of experimental methods that has been used to measure cavitation in HPH valves include free radical release and ultrasonic emissions (Floury et al., 2004; Håkansson et al., 2010; Kurzhals, 1977; Lander et al., 2000; Schlender et al., 2015; Shirgaonkar et al., 1998). Both measures are related to the intensity at which collapse occur rather than to how much vapour is accumulated in the device. Thus, there is a need for moving the discussion on cavitation in HPH valves from extent to intensity.

The precise definition of 'cavitation intensity' depends on the application. For example, when cavitation is used to oxidize pollutants

* Corresponding author.
E-mail address: andreas.hakansson@ple.lth.se (A. Håkansson).

https://doi.org/10.1016/j.ces.2025.121896
Received 26 March 2025; Received in revised form 5 May 2025; Accepted 19 May 2025
Available online 21 May 2025

Nomenclature

Abbreviations

ANN	Artificial neural network.
CFD	Computational fluid dynamics.
DNS	Direct numerical simulation.
HPH	High-pressure homogenizer.
TKE	Turbulent kinetic energy.

SymbolsLatin

f	Fanning's friction factor, –.
f_T	Turbulent fluctuation pressure frequency, Hz.
h	Gap height, m.
I_{cav}	Cavitation intensity, –.
k	Turbulent kinetic energy, $m^2\ s^{-2}$.
k_B	Kinetic energy at bubble collapse, m^2, s^{-2}.
K_{ex}	Exit pressure loss coefficient, –.
K_{gap}	Gap pressure loss coefficient, –.
K_{in}	Inlet pressure loss coefficient, –.
$L_{\bullet OH}$	Hydroxyl radical load, –.
l_B	Cavity collapse length scale, m.
L_g	Gap length, m.
n_{H_2O}	Number of water molecules (in the bubble), –.
n_{N_2}	Number of nitrogen molecules (in the bubble), –.
p_1	First stage pressure, Pa.
p_2	Backpressure (to first stage), Pa.
p_∞	Static pressure external to vapour bubble, Pa.
p_B	Bubble pressure, Pa.
p_{Blake}	Blake threshold pressure, Pa.
p_T	Turbulent fluctuation pressure amplitude, Pa.
p_{vap}	Vapour pressure, Pa.
$\overline{p}$	Time-average component of pressure, Pa.
P_{cav}	Cavitation performance
Q	Flowrate, $m^3\ s^{-1}$.
R_0	Initial gas bubble radius, m.
R_B	Bubble radius, m.
r_{ex}	Gap exit radius, m.
r_{in}	Gap inlet radius, m.
T	Temperature, K.
t	Time, s.
T_B	Bubble temperature, K.
Th	Thoma number ($=p_2/p_1$), –.
$\overline{u'}$	Mean turbulent velocity fluctuation, m s^{-1}.
U_{in} (U_{ex})	Gap inlet (exit) velocity, m s^{-1}.
v_B	Bubble collapse velocity, m s^{-1}.
$x_{\bullet OH}$	Mole fraction of hydroxyl radical, –.

Greek

γ	Interfacial tension (vapour bubble/liquid water), N m^{-1}.
Δp	Homogenization pressure, Pa.
ε_{cav}	Cavitation induced dissipation rate of kinetic energy, $m^2\ s^{-2}$.
ε_{turb}	Dissipation rate of TKE, $m^2\ s^{-2}$.
η_{cav}	Cavitation efficiency, –.
μ_C	Liquid viscosity, Pa s.
ρ_C	Liquid density, kg m^{-3}.
σ_{HPH}	HPH-cavitation number, –.
τ	Characteristic timescale of the jet, s.
ϕ_V	Volume average of vapour volume fraction, –.

in wastewater, the intensity is related to the generation of hydroxyl radicals (number, number density, rate, utilization etc). For emulsification applications, it is reasonable to relate cavitation intensity to the localised energy dissipation rate or shear generated due to collapsing cavities (Pandit et al., 2021; Ranade and Ranade, 2023; Sawant et al., 2008). In this work, we define the 'cavitation intensity' as the dissipation rate of energy due to vapour bubble collapse resulting from the implosion of a single cavity.

Despite a relatively large number of studies, there are several unanswered questions related to cavitation intensity in HPHs. One such question is how to understand the empirical observation that emulsion drop breakup is suppressed or delayed in HPHs subjected to extensive cavitation (Gothsch et al., 2015; Preiss et al., 2021; Schlender et al., 2015), when hydrodynamic cavitation is known to be an effective method to break emulsion drops in other devices (Carpenter et al., 2022; Gode et al., 2023; Perdih et al., 2010; Thaker and Ranade, 2022; Thaker and Ranade, 2023). Thus far, no convincing explanation has been offered.

Another challenge that is, arguably, related to the need to distinguish between cavitation extent and intensity in HPHs, is in understanding the effect of the main operating parameter of a HPH–the homogenizing pressure, Δp–on cavitation. As discussed in Part 1 of this series (Rütten and Håkansson, 2025), the cavitation number increases with homogenizing pressure if the Thoma number ($Th = p_2/p_1$) is kept constant. This is somewhat contra intuitive in the light of that many studies on the effects of cavitation in HPH valves (e.g., ultrasonic emissions, valve wear and free-radical formation) show an increase in cavitation with increased homogenization pressure (Floury et al., 2004; Håkansson et al., 2010; Håkansson, 2025; Innings et al., 2011; Kurzhals, 1977; Lander et al., 2000; Schlender et al., 2015, 2016; Shirgaonkar et al., 1998). In Part 1 (Rütten and Håkansson, 2025), we see that these measures of the cavitation extent (e.g., volume fraction of vapour accumulated in the valve) decreases with increased cavitation number, as expected. However, in this context, it is difficult to explain the empirical observations of increased cavitation with increasing homogenizing pressure. We argue that this discrepancy can be understood by distinguishing between cavitation extent and intensity.

To the best of the author's knowledge, there have been no attempt to model cavitation intensity in HPH valves. However, the HPH valve has many similarities to venturis, orifice, or vortex devices, which have been extensively studied (e.g., Chaudhuri and Chatterjee, 2024; Dastane et al., 2019; Ding et al., 2024; Hong et al., 2023; Li et al., 2025; Maleki et al., 2025; Simpson and Renade, 2018; Simpson and Renade, 2019; Yang et al., 2025). Moreover, in the more general literature on process intensification and cavitation, there exist a relatively mature methodology for estimating cavitation intensity (Chakma and Moholkar, 2013; Gogate and Pandit, 2000; Kumar et al., 2012; Moholkar and Pandit, 1997; Moholkar, 2001; Pandit et al., 2021; Pawar et al., 2017; Ranade and Ranade, 2023; Sawant et al., 2008; Simpson and Renade, 2018; Simpson and Renade, 2019). These studies use a single cavity model–based on a Keller-Miksis formulation (Keller and Miksis, 1980)–to predict the expansion and collapse of a single vapour bubble. The speed of the cavity wall collapse is used to estimate how fast energy is dissipated by the collapse event, and this dissipation rate is used to quantify the cavitation intensity (Sawant et al., 2008; Pandit et al., 2021; Ranade and Ranade, 2023).

The Keller-Miksis model also allows for the prediction of the temperature, pressure and molecular composition of the vapour bubble at the collapse. Mechanistically the process is complicated (Kalmár et al., 2022). However, previous studies have successfully used a simple 'hot-spot' theory in the prediction of free radical formation due to hydrodynamic cavitation (Chakma and Moholkar, 2013; Pandit et al., 2021; Pawar et al., 2017). According to this approach, the mole fraction of free radicals can be calculated from equilibrium theory (i.e., minimizing the

Gibbs free energy) at the maximum pressure and temperature inside of the bubble resulting from the implosion. The underlying assumption is that this chemical equilibrium sets in substantially faster than it takes for the vapour bubble to implode.

The abovementioned modelling approach to predict cavitation intensity and free radical release due to hydrodynamic cavitation has been seen to correlate well with experimental measures of cavitation intensity in previous studies (e.g., Ding et al., 2024; Hong et al., 2023; Sawant et al., 2008; Pawar et al., 2017). Thus, it is a promising approach that could also help to develop an understanding on cavitation intensity in the context of high-pressure homogenization.

The aim of this contribution is to extend the previously suggested method of modelling cavitation intensity to a HPH valve and combine it with the CFD-methodology used in the first part of this series (Rütten and Håkansson, 2025) to understand how operating parameters (homogenizing pressure and Thoma number) relate to cavitation intensity. More specifically, the research questions are:

- What similarities and differences are there between how cavitation extent and intensity depend on operating conditions in a HPH valve?
- Can the concept of cavitation intensity be used to understand the apparently contradictory finding that experimental studies observe an increase in cavitation with homogenizing pressure despite that this results in an increasing cavitation number?
- Can the concept of a cavitation intensity be used to better understand why extensive cavitation does not aid in drop breakup in HPHs?
- How well does the modelling framework explain empirical observations of how free radical formation in HPHs depend on operating conditions?

We have developed an approach and a framework to address these questions in the current contribution. The developed framework and results will be useful for optimising HPH as well as other hydrodynamic cavitation-based processes.

2. Theory and calculations

2.1. A modelling framework

As described above, this study applies and adopts a previously used modelling framework, based on single cavity collapse simulations, to predict the cavitation intensity in HPH valves, as a function of operating conditions. The modelling framework for calculating the cavitation intensity, ε_{cav}, –based on known information about the HPH valve geometry, operating conditions and fluid properties–is presented in Fig. 1 and summarized below: In the first step, a pressure drop correlation is used to estimate the primary hydrodynamic parameters of the valve (i.e., gap height and gap velocity). This is described in more detail in Section 2.2. In the second step, the parameters driving vapour bubble collapse (e.g.,

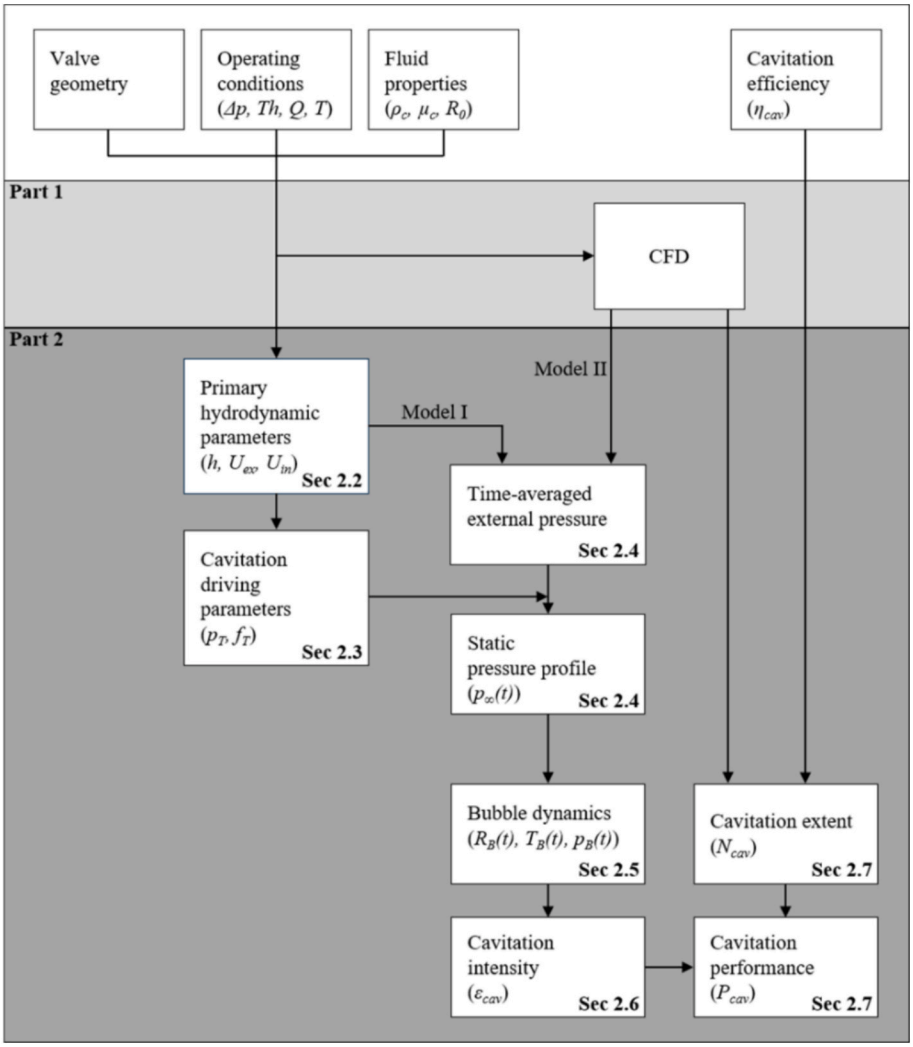

Fig. 1. Overview of the modelling framework suggested for predicting cavitation intensity from HPH valve geometry, operating conditions and fluid properties.

amplitude and frequency of pressure fluctuations) are estimated based on the primary hydrodynamic parameters (see Section 2.3). The static pressure profile (external to the bubble) is either estimated (simple and fast method, 'model I') or calculated based on two-phase CFD (presumably more representative, 'model II') (see Section 2.4). The next step in the modelling framework predicts the expansion and collapse of a vapour bubble subjected to such a pressure profile (see Section 2.5). This is used to calculate the dissipation created by a microjet implosion (see Section 2.6), which is identical to the cavitation intensity, ε_{cav}.

Note, however, that ε_{cav} is a measure of the intensity resulting from a single collapse. It needs to be combined with the number of cavities collapsing per unit volume (N_{cav}). N_{cav} is a measure of cavitation extent and can be estimated based on the quantities calculated in Part 1 of this series (Rütten and Håkansson, 2025), as described in Section 2.7. However, from a practical perspective, when attempting to understand and predict the effect of cavitation on, for example, wear or of cell breakup, it is important to note that all cavity implosions are not necessarily as effective. Implosions extort a powerful effect but are short-lived. Thus, how close to targets they occur are expected to play a role. Based on this line of argument, we propose that the cavitation performance of a device, P_{cav}, is modelled as the product of ε_{cav}, N_{cav} and an efficiency factor, η_{cav},

$$P_{cav} \propto N_{cav} \cdot \in_{cav} \cdot \eta_{cav} \tag{1}$$

The cavitation efficiency is likely to depend on which effect of the cavitation we study (i.e., wear or cell breakup). In this study, however, we simplify the model by setting $\eta_{cav} = 1$ throughout.

As mentioned in the introduction, several previous studies have quantified cavitation in HPHs from the release of free radicals. The cavity implosion framework is extended for predicting free radical performance in Section 2.8.

2.2. Pressure-drop correlation

The intensity of a HPH is controlled by varying the homogenizing pressure. Primary hydrodynamic parameters, such as gap velocities and gap height, can only be accessed indirectly, typically through solving for these quantities using pressure loss correlations (Håkansson, 2024; Phipps, 1975). In this study, we use a pressure loss correlation developed using an extensive CFD-campaign on HPH-valves operated to avoid cavitation. Results from that study suggested that the total homogenizing pressure, Δp, can be modelled as (Håkansson, 2024),

$$\Delta p = \Delta p_{ic} + \Delta p_{gap} + \Delta p_{oc} \tag{2}$$

$$\Delta p_{ic} = K_{in} \cdot \frac{\rho_C \cdot U_{in}^2}{2} \tag{3}$$

$$\Delta p_{gap} = K_{gap} \cdot 4f(Re_{ex}) \cdot \frac{L_g}{2h} \cdot \frac{\rho_C \cdot U_{ex}^2}{2} \tag{4}$$

$$\Delta p_{oc} = K_{ex} \cdot \frac{\rho_C \cdot U_{ex}^2}{2} \tag{5}$$

with K_{in}, K_{gap} and K_{ex} being Reynolds number dependent friction loss coefficients (see the original study for explicit expressions) and f being Fanning's friction coefficient. In addition to Eqs. (2)–(5), mass preservation (assuming constant fluid densities) relates flowrate to gap velocities and gap-height:

$$Q = 2\pi \cdot U_{in} \cdot r_{in} \cdot h = 2\pi \cdot U_{ex} \cdot r_{ex} \cdot h \tag{6}$$

Provided a valve geometry (i.e., r_{ex}, r_{in} and L_g), fluid properties (ρ_C, μ_C), and the operating conditions (Q and Δp), the gap-height and gap-velocities were calculated by numerically solving Eqs. (2)–(6) using a derivative free numerical nonlinear equation solver implemented in MATLAB R2022a (MathWorks, Natick, MA) as the built-in function 'fzero'.

In Part 1 of this series (Rütten and Håkansson, 2025), it was seen that this pressure loss correlation gives less than a 5 % error under mildly cavitating conditions. The error increases somewhat with more extensive cavitation but is never more than 15 %.

All investigations of the present study are based on the HPH valve described in the first part of this series (Rütten and Håkansson, 2025), i.e., $r_{ex} = 2.3$ mm, $L_g = 0.5$ mm, $Q = 250$ L/h, $\rho_C = 1010$ kg/m^3, $\mu_C = 0.6$ mPa s.

2.3. Bubble implosion driving quantities

Previous investigations have identified the instantaneous static pressure profile in general, and the amplitude and frequency of turbulence-induced pressure fluctuations in particular, to be of critical importance for understanding the expansion and implosion of cavitation bubbles in turbulent flows (Moholkar and Pandit, 1997; Pandit et al., 2021; Pawar et al., 2017; Ranade and Ranade, 2023).

Detailed information on the instantaneous pressure external to the bubble, the amplitudes or frequencies, and how they depend on operating parameters, would require a large direct numerical simulation (DNS) campaign. Whereas we have previously performed DNS on simplified valves (Olad et al., 2022a; Olad et al., 2022b), it is still too computationally expensive for industrially relevant HPH valves. The situation is similar for other devices. Therefore, previous studies use correlations based on more readily accessible parameters to describe the instantaneous pressure variations driving bubble expansion and collapse (Moholkar and Pandit, 1997; Pandit et al., 2021; Pawar et al., 2017; Ranade and Ranade, 2023).

The instantaneous pressure instantaneous static pressure experienced by the bubble, $p_\infty(t)$, is modelled as the sum of a time-averaged component, $\overline{p}(t)$, and a sinusoidal fluctuation (Moholkar and Pandit, 1997; Pandit et al., 2021; Pawar et al., 2017; Ranade and Ranade, 2023):

$$p_\infty(t) = \overline{p}(t) + p_T \cdot \sin(2\pi \cdot f_T \cdot t) \tag{7}$$

To ensure that the instantaneous pressure is physically realistic, a minimum value of 0 Pa is set on $p_\infty(t)$.

The amplitude of pressure fluctuations, p_T, is typically found to be proportional to fluid density and the turbulent kinetic energy. Following Pawar et al. (2017) and Moholkar (2001), we estimate,

$$p_T = \rho_C \cdot k \tag{8}$$

The frequency of pressure fluctuations, f_T, is modelled as the characteristic velocity fluctuation divided by the length-scale of the largest turbulent eddies (Moholkar and Pandit, 1997). For the outlet chamber of a HPH, the integral length-scale of turbulent eddies is approximately equal to three gap heights (Innings and Trägårdh, 2007). Assuming isotropic turbulence, the average of the velocity fluctuations can be estimated from the turbulent kinetic energy,

$$\overline{u'} = \sqrt{2/3} \cdot k^{1/2} \tag{9}$$

and therefore,

$$f_T = \frac{\overline{u'}}{3 \cdot h} = \frac{\sqrt{2/3} \cdot k^{1/2}}{3 \cdot h} \tag{10}$$

Eqs. (8) and (10) suggest that both the amplitude and the frequency of pressure fluctuations can be estimated from gap height (h) and TKE (k). The former is obtained as described in Section 2.2. Generally, the TKE of a turbulent jet is expected to be proportional to the square of the jet velocity (i.e., U_{ex} in the HPH) with a proportionality constant of order magnitude 0.01–0.1 (Pope, 2000, pp. 134). From carrying out a range of CFD simulations with varying gap-heights (see Supplement S.1), it is concluded–empirically–that the following scaling is appropriate for the HPH valve:

$$k = 0.025 \cdot U_{ex}^2 \tag{11}$$

2.4. Static pressure profiles outside of the bubble

The methodology of approximating the instantaneous pressure external to the bubble with a sinusoidal model (e.g., Eq. (7)) has been widely adopted in previous studies. However, the previous studies differ in how the time-averaged pressure, $\bar{p}(t)$, is modelled. In this contribution, two different approaches were used. By comparing results from these two approaches, we perform a sensitivity analysis, helping to ensure model validity. Moreover, this allows us to test the suitability of the simpler approach. The first approach (Moholkar and Pandit, 1997; Pandit et al., 2021; Pawar et al., 2017), approximates $\bar{p}(t)$ with a linear profile, increasing from the vapour pressure, p_{vap}, to the downstream pressure (i.e., p_2, the backpressure to the valve, in the present study), with a time-constant τ.

$$\bar{p}(t) = \begin{cases} p_{vap} + t \cdot \dfrac{p_2 - p_{vap}}{\tau} & t \le \tau \\ p_2 & t > \tau \end{cases} \tag{12}$$

The rational for setting the starting point at p_{vap} is that this is where the bubbles start expanding, and, thus, the implosion will occur downstream of this point.

The time-constant, τ, is estimated as the time required to travel 15 gap height in the outlet chamber jet downstream of the gap exit,

$$\tau = \frac{15 \cdot h}{U_{ex}} \tag{13}$$

Using the simplified profile (Eq. (12)) for estimating the time-averaged pressure will be referred to as employing 'model I' below (see Fig. 1). The advantage with this approach is that it allows for calculation of the cavitation intensity (as well as free radical formation) directly from geometry, fluids and operating conditions, without having access to CFD.

The second approach (Dastane et al., 2019; Hong et al., 2023; Simpson and Renade, 2018; Simpson and Renade, 2019) is to estimate $\bar{p}(t)$ from the static pressure on discrete particle model (DPM) trajectories calculated based on a CFD model of the cavitating flow. In the current study, 200 inert 1 μm diameter spherical particles were released in the steady-state CFD solution from part one of this series (Rütten and Håkansson, 2025). Trajectories were initiated at the gap inlet, 1/10 of the gap-height distance from the seat wall. This corresponds to the position of maximum local evaporation rate according to the macroscopic Schnerr-Sauer cavitation model (Rütten and Håkansson, 2025). The particle trajectories were calculated taking virtual mass and pressure gradient forces into account and using a stochastic tracking method with an eddy lifetime given by 0.15 times the (local) TKE divided by the dissipation rate of TKE (Simpson and Renade, 2018; Simpson and Renade, 2019). All DPM trajectories were obtained via the discrete particle tracking module in Fluent 2019R1 (ANSYS, Canonsburg, PA).

Note that each operating condition (i.e., each combination of Δp and Th), gives rise to 200 trajectories. For each such trajectory, $p_\infty(t)$ was calculated using Eq. (7). This was, subsequently, used to calculate bubble dynamics and cavitation-induced energy dissipation (see subsections below). The average across all 200 trajectories was used to characterize each operating condition.

The use of steady-state CFD to calculate the DPM for calculating the time-averaged pressure is an approximation that, substantially, reduced computational cost. A sensitivity analysis was performed by repeating the DPM-analysis on three transient CFD-solutions to one of the cases (Th = 1 %, Δp = 26 MPa), collected at between 0 and 3500 μs from departing from the steady-state solution. Each of the three sets of DPM-solutions was used to calculate the cavitation intensity (see Sections 2.5-2.6). The calculated average cavitation intensities (across the trajectories) were not identical, but similar (i.e., $1.37 \cdot 10^6$ m^2/s^3, $1.15 \cdot 10^6$ m^2/s^3 and $1.52 \cdot 10^6$ m^2/s^3). Thus, a steady-state CFD approach was adopted throughout the study.

2.5. Bubble dynamics

The Keller-Miksis equation (Keller and Miksis, 1980), with a van der Waal equation of state, a water vapour mass transfer closure model, and a pseudo steady state heat transfer model was used to calculate the evolution of the vapour bubble radius, R_B, the bubble temperature, T_B, the bubble pressure, p_B, the number of nitrogen molecules, n_{N_2}, and the number of water molecules, n_{H_2O}, as functions of time, t, given the external pressure profile, $p_\infty(t)$. A full description of model equations can be found in Pandit et al. (2021). To avoid implementation errors as well as to ensure a high degree of traceability, the MATLAB-based single cavity model (SCM) (https://github.com/AjinkyaPandit/cavitating-single-bubble) provided by Pandit et al. (2021) was used with minimal modifications. To adopt it to the current study, however, the SCM was lightly rewritten to allow it to operate without interfacing spreadsheets for parameter settings and pressure profiles. Following Pandit et al. (2021), both relative and absolute tolerances to the ordinary differential equation solver were set to 10^{-5}.

2.6. Cavitation intensity

The dissipation rate of kinetic energy due to cavitation implosions (i.e., the cavitation intensity) was estimated based on the approach suggested by Sawant et al. (2008). First, the radial liquid velocity at the collapsing bubble was estimated from the bubble dynamics:

$$v_B(t) = \left|\frac{dR_B}{dt}\right| \cdot \left(\frac{R_B(t)}{R_{B,max}}\right)^2 \tag{14}$$

The first temporal derivative of $R_B(t)$ was calculated using a five-point stencil (Sauer, 2012).

Secondly, the eddy length-scale associated with the cavity collapse oscillation, l_B, was estimated as the time-averaged bubble radius (calculated using a trapezoidal rule integration, using the function 'trapz' as supplied in MATLAB R2022a) (Sawant et al., 2008). Third, the kinetic energy (per mass) arising from the microjet resulting from an implosion was estimated from that velocity (Sawant et al., 2008),

$$k_B(t) = 0.5 \cdot v_B^2(T) \tag{15}$$

and, finally, the dissipation rate of cavitation implosion energy was calculated from velocity scale cubed, divided by length-scale (assuming a proportionality constant of one) (Sawant et al., 2008), i.e.,

$$\epsilon_{cav}(t) = \frac{k_B^{3/2}(t)}{l_B} \tag{16}$$

Following Sawant et al. (2008), the characteristic ε_{cav} was calculated from taking the average of the time-dependent expression in Eq. (16) over the 'lifetime of the cavity' (Sawant et al., 2008, p. 324), which in this study is interpreted as when $R_B(t) > 1.05\ R_0$.

2.7. Cavitation extent and performance

As discussed above (Eq. (1)), we define cavitation performance as the product of the cavitation intensity, the number density of cavities and an efficiency factor (arbitrarily set to one in this study).

The number density of cavities (number per unit volume) was estimated from assuming that, initially, there are N_{cav} cavities all with radius R_0 and that the volume fraction of vapour is ϕ_v,

$$N_{cav} = \phi_v \cdot \frac{3}{4\pi \cdot R_o^3} \tag{17}$$

The volume fraction in the device is heterogenous (Rütten and Håkansson, 2025), and there are different options for how to model ϕ_v. A straight-forward approach is to identity ϕ_v with the volume integral average over the valve. The first part of this series (Rütten and Håkansson, 2025), showed that the volume average integral of the

vapour volume fraction is a function of the cavitation number. It can be, empirically, modelled (see Supplement Section S.2 for a motivation) as,

$$\phi_v = \begin{cases} 0.13 \cdot \exp(-56 \cdot \sigma_{HPH}) if \sigma_{HPH} < 0.20 \\ 0 else \end{cases} \quad (18)$$

The second row in Eq. (18) models that cavitation is supressed at sufficiently high cavitation numbers, i.e., if $\sigma_{HPH} > 0.20$ according to Part 1 of this series (Rütten and Håkansson, 2025). The HPH cavitation number is defined,

$$\sigma_{HPH} = \frac{p_2 - p_{vap}}{0.5 \cdot \rho_C \cdot U_{in}^2} \quad (19)$$

and is readily calculated (for set of each operating conditions) based on the primary hydrodynamic parameters calculated from Section 2.2.

However, estimating the number of cavity collapses based on the volume average of vapour might be questioned. If the volume fraction of vapour is close to one (i.e., a vapour filled region), this is more likely to give rise to a hydraulic flip (Schlender et al., 2015) than a large number of cavity collapses. Thus, as a sensitivity analysis, we compare the method above to estimating ϕ_v as the volume fraction of the device with a vapour volume fraction between 10 % and 50 %. This range aims to capture the regions where cavity collapses are expected. The comparison showed that the two approaches resulted in a nearly identical estimation of ϕ_v (see Section S.3 in the Supplement). Thus, the volume average (Eq. (18)) was used in the rest of the study.

2.8. Free radical formation

Cavitation gives rise to the formation of free radicals. This has often been used to quantify cavitation in HPHs (Floury et al., 2004; Gogate et al., 2021; Lander et al., 2000; Shirgaonkar et al. 1998). Following previous investigations (Chakma and Moholkar, 2013; Ding et al., 2024; Li et al., 2025; Pandit et al., 2021; Pawar et al., 2017), we use the 'hot spot' theory to predict the release of free radicals in the present study. The Equilib software in FactSage 8.3 (Bale et al., 2009) is used to solve the Gibbs free energy minimization problem. The gas bubble is assumed to consist of nitrogen and water vapour, the relative amounts are obtained from the bubble dynamics model (see Section 2.5).

The minimization of Gibbs free energy, results in an estimation of the mole fraction of all chemical species created in the implosion, including the free radicals. Previous studies suggest the hydroxyl radical (Chakma and Moholkar, 2013; Pawar et al., 2017), •OH, to be the dominating species, and this is also confirmed in the present study. Thus, the current study reports results as the mole fractions of •OH, $x_{\bullet OH}$. However, note that $x_{\bullet OH}$ describes the effect of a single vapour bubble. To obtain an indicator representative of what is obtained in the experimental studies, the free radical performance; $P_{\bullet OH}$, is defined as the mole fraction multiplied with the number density of cavitation bubbles and an efficiency factor,

$$P_{\bullet OH} = x_{\bullet OH} \cdot N_{cav} \cdot \eta_{cav,\bullet OH} \quad (20)$$

In analogy with the discussion in Section 2.1, the efficiency factor is assumed to be equal to one, for simplicity.

3. Results and discussion

3.1. Effect of operating parameters on HPH hydrodynamics

HPHs are designed to rapidly dissipate turbulent kinetic energy in a small region downstream of the gap exit (Håkansson, 2019). The increased hydrodynamic intensity resulting from operating a HPH at an increased homogenizing pressure, comes from a reduction in the gap height and an increase in gap velocities, leading to an increase in the dissipation rate of TKE. This is illustrated in Fig. 2 for the case of a HPH with a gap exit diameter of 4.6 mm, a gap length of 0.5 mm, a flowrate of 250 L/h, and run with water at 25 °C. Note that the back-pressure ratio ($Th = p_2/p_1$) does not influence gap height or gap velocities (if the homogenizing pressure is kept constant). Also note that the velocity at the gap inlet, U_{in}, is larger than at the gap exit, U_{ex}, due to the area expansion effect of a radial diffuser HPH valve.

Fig. 3 displays the resulting effect on the amplitude and frequency of pressure fluctuations from varying homogenizing pressure and Thoma number (calculated as described in Section 2.3). First note that the amplitude of pressure fluctuations increases almost linearly with homogenizing pressure but is independent of Thoma number (Fig. 3A and C). This is expected from that TKE increases and gap-height decreases as homogenizing pressure is increased (whereas none of the parameters depend on Thoma number), as seen from Eq. (6). A similar increase can be seen in the frequency of pressure oscillations (Fig. 3B and D).

Also note that both amplitude and frequency of pressure fluctuations are large in comparison to previously studied systems such as vortex generators and venturis (Pandit et al., 2021; Sawant et al., 2008; Simpson and Renade, 2018; Simpson and Renade, 2019)—amplitudes reach 2–10 MPa and frequencies of 100–450 kHz. This is expected since the HPH (in contrast to these other devices) is designed with the main purpose of delivering intense turbulence. Thus, the TKE is high which results in high values of p_T and f_T (see Eqs. (8) and (10)).

3.2. Blake threshold pressure as a criterion for cavitation implosions

A vapour bubble subjected to a pressure amplitude exceeding the Blake threshold pressure, p_{Blake}, will grow and/or shrink uncontrollably (Harkin et al., 1999). Consequently, a pressure amplitude exceeding p_{Blake} has been suggested as a necessary and sufficient condition for

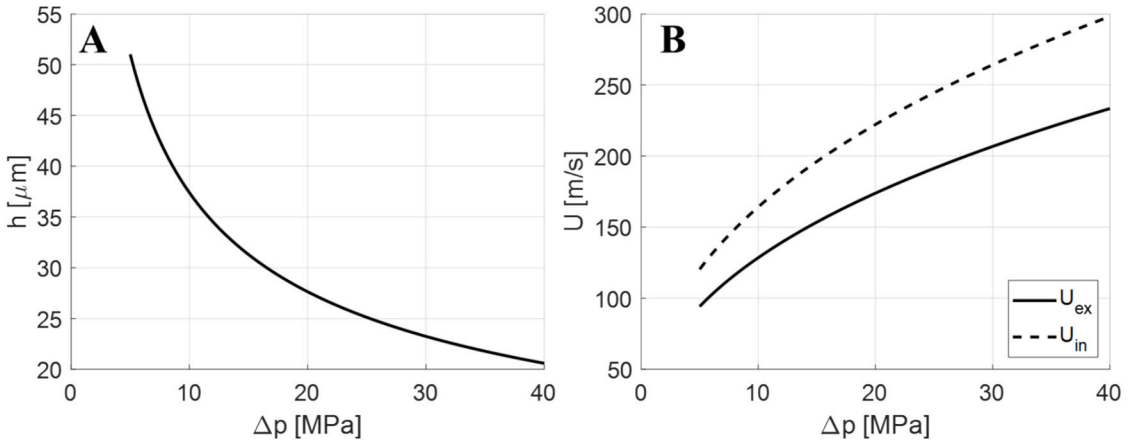

Fig. 2. Gap-height (A) and gap velocities (B, solid line: gap exit velocity, dashed line: gap inlet velocity). For valve geometry and fluid properties, see Section 2.2.

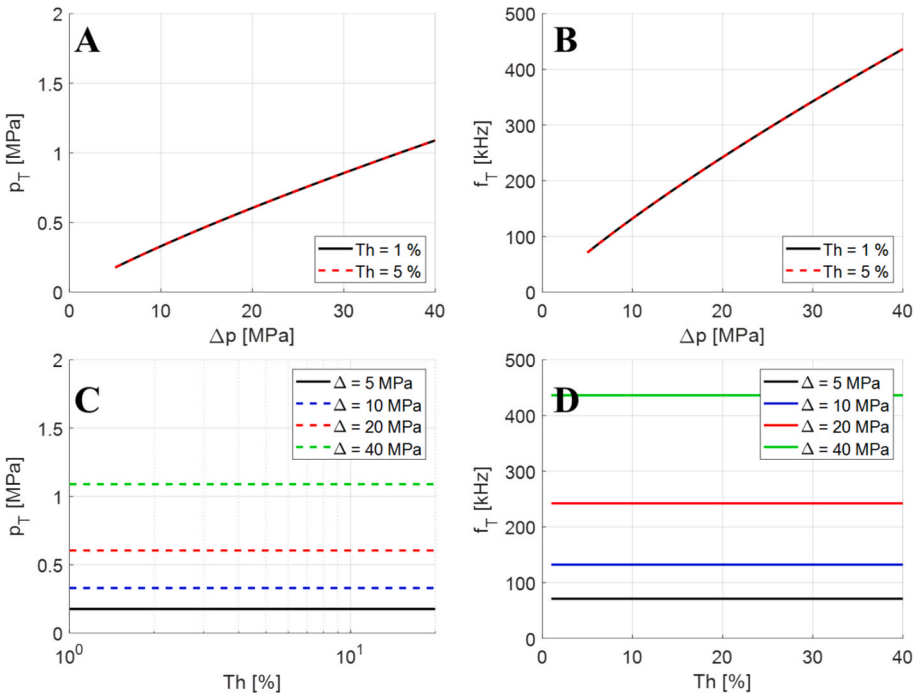

Fig. 3. Cavitation driving parameters plotted as functions of homogenizing pressure (A and B), Δp, and Thoma number, Th (C and D). A,C) Turbulent pressure fluctuation amplitude, p_T. B,D) Turbulent pressure fluctuation frequency f_T.

cavitation implosions to occur (Pandit et al. 2017, p. 8). For a HPH, the pressure far downstream of the cavitating region is represented by the backpressure, p_2, and thus:

$$p_{Blake} = p_2 - p_{vap} + \sqrt{\frac{32 \cdot \gamma^3}{27 \cdot R_0^3 \cdot \left(p_2 - p_{vap} + 2\gamma/R_0\right)}} \tag{21}$$

Note that the Blake threshold depends on the radius of the initial gas bubble (R_0). An illustration is provided in Fig. 4 (with $\gamma = 72$ mN/m). Also note that if the initial vapour bubble radius is large (i.e., $R_0 > 1$ μm), Eq. (21) results in $p_{Blake} \approx p_2$. If the initial gas bubble is substantially smaller than this, the bubble can keep from going into a violent expansion and/or collapse at substantially higher pressure amplitudes. Moreover, this effect becomes more pronounced the lower is the homogenizing pressure (Fig. 4A) and the lower is the Thoma number (Fig. 4B).

Fig. 5 displays the ratio between pressure amplitude and Blake pressure as a function of homogenizing pressure (at Th = 1 %) (Fig. 5A) and Thoma number (at $\Delta p = 20$ MPa) (Fig. 5B). Starting with Fig. 5A, note that at this low Thoma number (Th = 1 %), the pressure amplitude greatly exceeds the Blake threshold pressure if R_0 is not much smaller than 1 μm. This suggests that violent vapour bubble collapse will occur regardless of the homogenizing pressure applied. However, as seen in Fig. 5B, as soon as a relatively low backpressure is applied, this substantially reduces the Blake threshold pressure (note that $p_{Blake} \approx p_2$), so that the ratio falls below the critical limit of $p_T/p_{Blake} = 1$. The lowest Thoma number required to keep $p_T/p_{Blake} < 1$ (i.e., to supress cavitation according to this prediction method), is 2.8–3.0 % (if $R_0 \leq 1$ μm). If the initial gas bubble diameter is smaller still, the Blake threshold suggest that no implosions will occur even if the Thoma number is as low as 1 %. The critical Thoma number depends very weakly on the applied homogenizing pressure, i.e., at $R_0 = 1$ μm, the critical Th is in the range 2.5–3.0 % when 5 MPa $< \Delta p <$ 40 MPa (results not shown).

Although the size of the initial gas bubble in a typical case of high-pressure homogenization is unknown, the proceeding analysis is carried out assuming $R_0 = 1$ μm. This choice is made partially based on that the bubble dynamics appears relatively insensitive to variations in R_0 above this limit, and partially due to that a substantially smaller R_0 appears unrealistic in the light of Fig. 5B and previous empirical observations of cavitation sound, wear and free radical formation, show cavitation taking place at Thoma numbers well above Th = 1 % (Floury et al., 2004; Håkansson, 2025; Håkansson et al., 2010; Lander et al.,

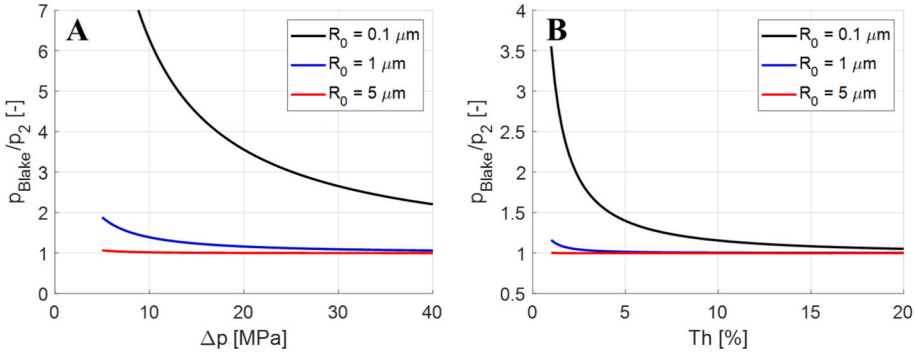

Fig. 4. Blake threshold pressure, p_{Blake}, normalized to the backpressure, p_2, as a function of homogenizing pressure (at Th = 1 %) (A) and Thoma number (at Δp = 20 MPa) (B). Results displayed for three values of $R_0 = 0.1$ μm (black line), $R_0 = 1$ μm (blue line) and $R_0 = 5$ μm (red line).

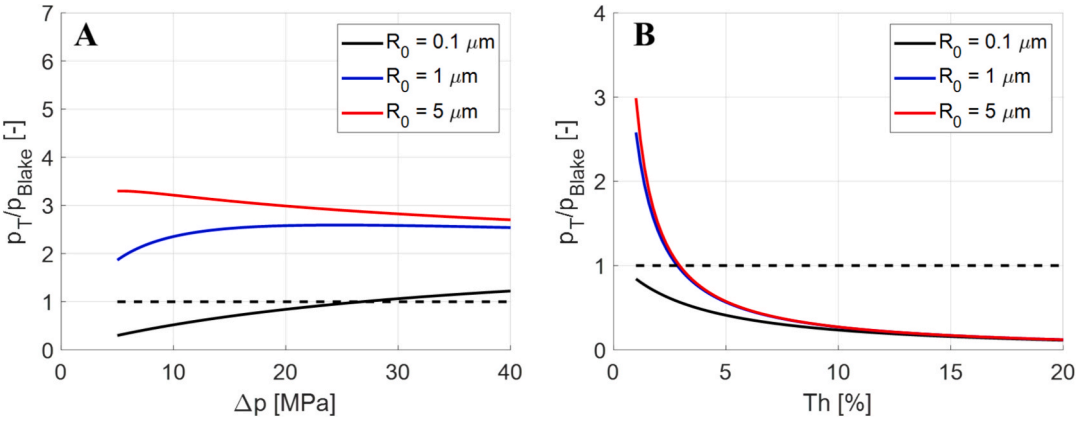

Fig. 5. Blake threshold analysis, showing the operating conditions where the pressure amplitude, p_T, is larger than the Blake threshold pressure, p_{Blake}, and thus, where cavity collapse is expected. A) p_T/p_{Blake} as a function of homogenizing pressure. B) p_T/p_{Blake} as a function of Thoma number. Results displayed for three values of R_0 = 0.1 μm (black line), R_0 = 1 μm (blue line) and R_0 = 5 μm (red line).

2000; Shirgaonkar et al., 1998).

3.3. *Effect of homogenizing pressure on bubble collapse and cavitation intensity*

As discussed in Sections 2.4–5, a model of bubble collapse is obtained by solving the bubble dynamics Keller-Miksis equation. Model I assumes that the instantaneous external pressure follows a linearly increasing profile (from $p = p_{vap}$ to $p = p_2$, during a time-period τ), overlayed by a modelled pressure fluctuation (Eq. (7)). This closely followed the approach suggested in several previous studies (e.g., Moholkar and Pandit, 1997; Pandit et al., 2021; Pawar et al., 2017).

Fig. 6A displays the resulting pressure profiles at three different homogenizing pressures (Δp = 5 MPa, 22 MPa and 40 MPa) (based on using model I). Note the increase in both amplitude and frequency with increasing homogenizing pressure. Also note that the fluctuating pressure amplitude is large in relation to p_{vap} and p_2, and, thus, $p_\infty(t)$ is almost completely dominated by the fluctuating component.

Fig. 6B and C display the bubble diameter and temperature obtained from solving the Keller-Miksis equation (Section 2.5). Note that, regardless of homogenizing pressure, the bubble undergoes a sequence of dampened oscillations each linked to a violent collapse. For a short time-period during the collapse, the local bubble temperature increases to ~6000 K (relatively independently of homogenizing pressure, see Fig. 6C).

Fig. 6D–F compare the abovementioned results to those obtained using the trajectory-analysis for estimating the time-averaged component of the external pressure (i.e., model II). The lines display the maximum external pressure (Fig. 6D), bubble radius (Fig. 6E), and bubble temperature (Fig. 6F) over the first 20 μs based on using model I and the markers display the same data for model II (showing average plus/minus standard deviation across the 200 trajectories). As seen in

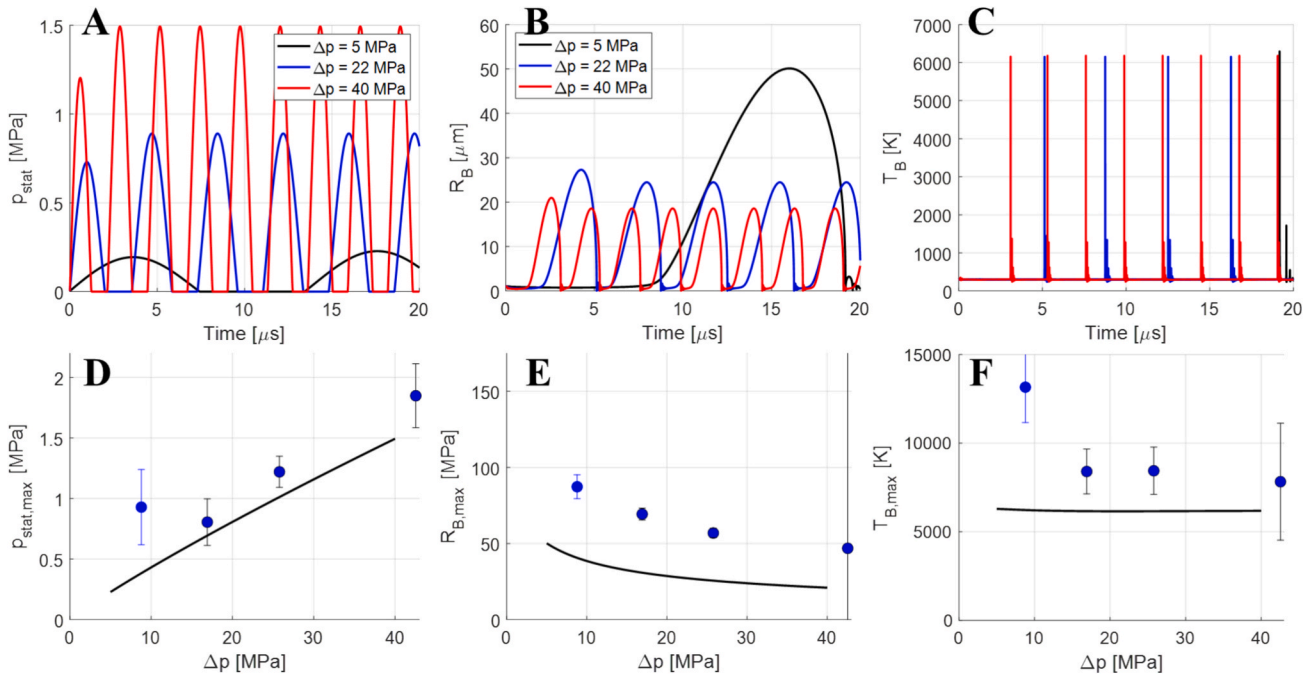

Fig. 6. A) External static pressure fluctuations (model I) at three different homogenizing pressures. The resulting bubble radius, R_B, and bubble temperature, T_B. are displayed in (B) and (C), respectively. D-F display the maximum static pressure (D), bubble radius (E), and bubble temperature (F), comparing the two approaches to model the time-averaged external pressure–the solid line displays results from model I and the solid markers display results from model II (average ± standard deviation across 200 trajectories). (Results obtained for R_0 = 1 μm, Th = 1 %).

the figure, the trends with respect to homogenizing pressure are similar.

The cavitation intensity, defined as the microjet energy dissipation associated with bubble collapse, can be seen in Fig. 7A (calculated as described in Section 2.6). The solid black line displays the predictions using the simplified pressure profile (model I), and the blue markers display the results from using the CFD-calculated pressure profiles (model II). Note that the estimates differ by several orders of magnitude (due to the inherent sensitivity of the bubble dynamics to small pressure variations). However, the trend is similar–ε_{cav} increases with homogenizing pressure at a diminishing rate.

As a further comparison, a dissipation rate of cavitation implosion energy prediction based on the artificial neural network (ANN) trained in a previous study (Ranade and Ranade, 2023) has also been inserted (dashed line). As seen in the figure, the ANN overpredicts ε_{cav} compared to the direct use of bubble dynamics simulations (solid lines). However, the ANN predicts the trend with increasing homogenizing pressure relatively well. This is surprising given that the ANN was trained on parameters corresponding to devices with substantially lower turbulence intensities. Thus, the parameters of the HPH valve are far outside the ones used for training the ANN (e.g., $f_T = 100$–450 kHz in this study, see Fig. 3B, whereas the ANN was trained on $f_T = 5$–80 kHz).

Fig. 7B displays the cavitation performance (modelled as the product of ε_{cav} and the number frequency of vapour bubbles, see Section 2.7). Note that, regardless of if using model I, model II or the ANN, the cavitation performance increases with homogenizing pressure. Moreover, P_{cav} increases somewhat steeper with homogenizing pressure than ε_{cav}.

Summarizing the findings thus far: regardless of which method that is used to estimate the time-averaged pressure, ε_{cav} and P_{cav} increase with homogenizing pressure. This implies that vapour bubble collapse is more violent the higher is the applied homogenizing pressure. This is a promising feature of the model in the light of the empirically observed increase in cavitation intensity with increasing homogenizing pressure (Floury et al., 2004; Håkansson et al., 2010; Innings et al., 2011; Kurzhals, 1977; Lander et al., 2000; Shirgaonkar et al., 1998). Also, note that this is a behaviour that could not be captured by a CFD coupled to a macroscopic cavitation model, or a description purely based on the cavitation number, since the cavitation number increases with increasing homogenizing pressures–see discussion in Part 1 of this series (Rütten and Håkansson, 2025).

It is also interesting to compare ε_{cav} to the characteristic turbulent dissipation rate of TKE from the outlet chamber turbulence, ε_{turb}. The dependence of ε_{turb} on the primary hydrodynamic variables of a HPH (in the absence of cavitation) has been studied to some extent, for example using DNS (Olad et al., 2022a, 2022b). These previous studies show that a good approximation of the ε_{turb} in the region where drop breakup takes place is,

$$\epsilon_{turb} = \frac{1}{140}\frac{U_{ex}^3}{h} \tag{22}$$

As seen in Fig. 7A, for the HPH, ε_{turb} is substantially larger than ε_{cav} (i.e., either a factor 10^2 or a factor 10^4 higher, depending on which of the pressure profile models that is used). This contrasts with flow devices where drop breakup is due to cavitation bubble implosions (Gode et al., 2023; Perdih et al., 2010; Thaker and Ranade, 2022; Thaker and Ranade, 2023). (Also note that the alternatives to Eq. (22) that have been suggested in other studies (Innings and Trägårdh, 2007), have a larger proportionality constant, which would lead to the conclusion of an even larger difference between ε_{turb} and ε_{cav}.) Again, this could be expected from that a HPH is designed to deliver intense turbulence as opposed to the previously mentioned devices, which are typically designed to effectively subject the fluid to cavitation.

The finding in Fig. 7A helps to explain why emulsion drop breakup is not aided by the presence of cavitation, as seen in visualization experiments for HPHs (Gothsch et al., 2015; Preiss et al., 2021); even if operating at virtually no backpressure, the cavitation implosions will not give rise to an as forceful disrupting force as the turbulent eddies. In a situation where even emulsion drops following trajectories taking them very close to a vapour bubble implosion will not experience a higher stress from this than from turbulent eddies, we do not expect cavitation to aid breakup.

As mentioned above, it has also been observed experimentally that extensive cavitation hinders breakup in scaled-up HPH valves (Gothsch et al., 2015, 2016; Preiss et al., 2021). This has been explained in terms of extensive cavitation influencing drop breakup via its effect on the macroscopic flow, for example Preiss et al. (2021) suggested that the presence of vapour weakens turbulence vortices. In the light of the observations in Part 1 of this series, another possible mechanism can be found in the effect extensive cavitation has on the jet orientation (Rütten and Håkansson, 2025). Both these hypotheses are consistent with the low cavitation induced dissipation rate of kinetic energy.

3.4. Effect of Thoma number on bubble collapse and cavitation intensity

Turning to the effect of Thoma number on the cavitation intensity, Fig. 8 displays the pressure profiles (using model I) and the corresponding bubble radius and bubble temperature plots. As noted above,

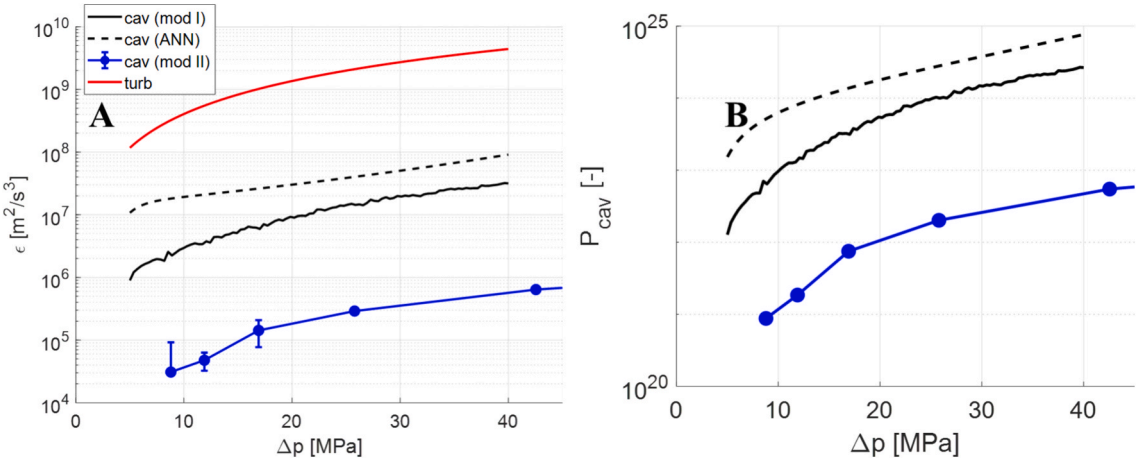

Fig. 7. A) Cavitation intensity (black and blue), compared to the dissipation rate of TKE in the HPH jet (red), as a function of homogenizing pressure, Δp. B) Cavitation performance (Eq. (16)) as a function of homogenizing pressure, Δp. For cavitation, the figure compares results from using a simplistic pressure profile (model I, black solid line), based on the CFD-trajectory pressure profiles (model II, blue markers), and a previously suggested ANN model (Ranade and Ranade, 2023) (dashed black line).

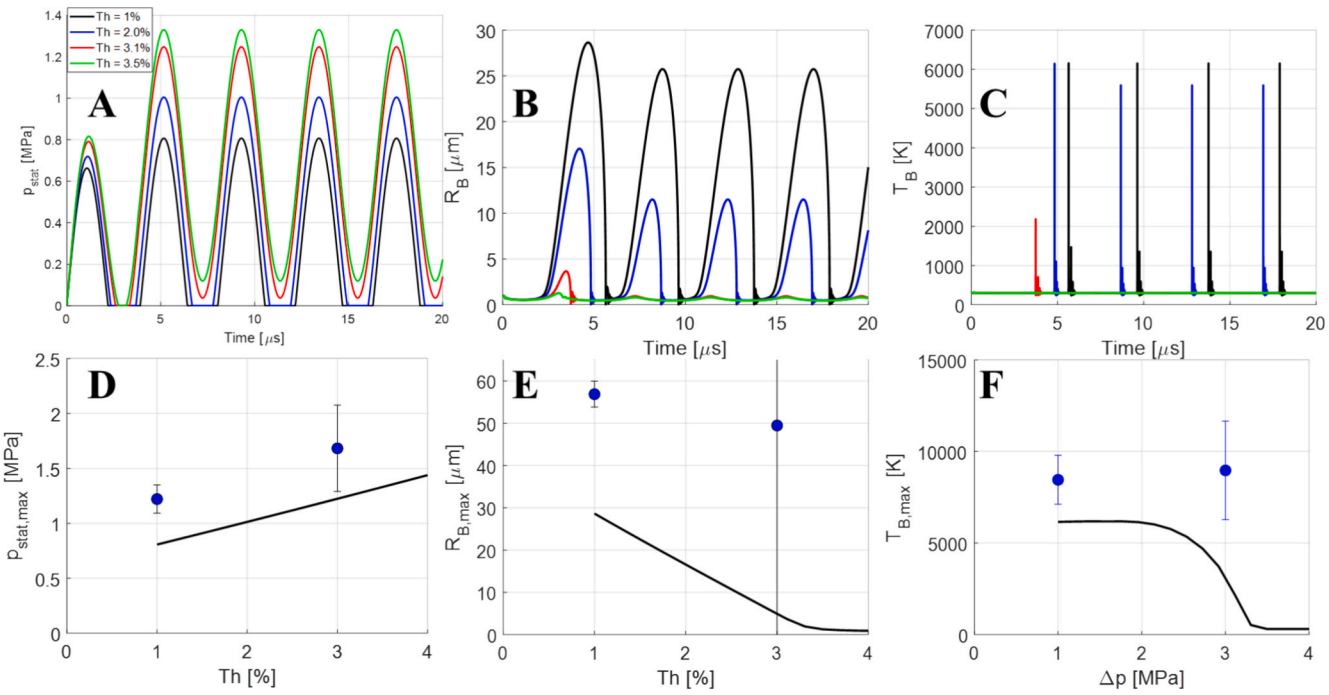

Fig. 8. The effect of Thoma number on bubble dynamics. A) Static pressure external to the bubble, p_∞, as a function of time. B) Bubble radius, R_B. C) Bubble temperature, T_B. Pressure profiles in (A-C) are generated with model I. (D-F) show the maximum external pressure (D), bubble radius (E) and bubble temperature (F), comparing model I (solid line) to model II (solid markers) (showing average ± standard deviation across 200 trajectories). (Results obtained for Δp = 26 MPa, R_0 = 1 μm.)

the external pressure profiles in Fig. 8A are dominated by the fluctuations (i.e., p_{vap} and p_2 are small in relation to p_∞). Fig. 8A also shows that the main effect of operating at a higher *Th* is to lift the pressure profile to a higher level. As seen in Fig. 8B, this results in a less violent collapse at higher Thoma numbers (i.e., smaller bubble radius amplitudes and larger temporal gradients of R_B). Note, however, that the span of Thoma numbers displayed in Fig. 8 is limited. As seen already in Section 3.2, applying a higher Thoma number than ~3 % leads to that no violent bubble implosion occurs (at least under the assumption that model I describes the external pressure profile). The same trend can be seen when inspecting the bubble temperature in Fig. 8C; the maximum temperature decreases rapidly when operating at higher Thoma numbers, until at Th = 3.5 %, temperature inside the bubble never exceeds 30 °C.

Fig. 8D–F shows a comparison between maximum external pressure (Fig. 8D), maximum bubble radius (Fig. 8E), and maximum bubble temperature (Fig. 8E), comparing results from the two approaches to modelling the time-averaged pressure–solid lines display model I and markers display model II (average ± standard deviation across 200 trajectories). As seen in Fig. 8D–F, the trends with Thoma number are similar.

Fig. 9A displays the corresponding cavitation intensity, ε_{cav}, as a function of Thoma number. The solid black line displays the estimates from the simplified linear pressure model (model I), corresponding to Fig. 8A–C. Note that only conditions where a catastrophic implosion collapse occurs (i.e., Th = 3.1 % but not Th = 3.5 in Fig. 8) are included (cf. Pandit et al., 2017). Also note that ε_{cav} increases somewhat with Thoma number, reaching a critical value below which $\varepsilon_{cav} \to 0$. This maximum is possibly due to that the difference between the maximum and minimum external static pressure experienced by the bubble

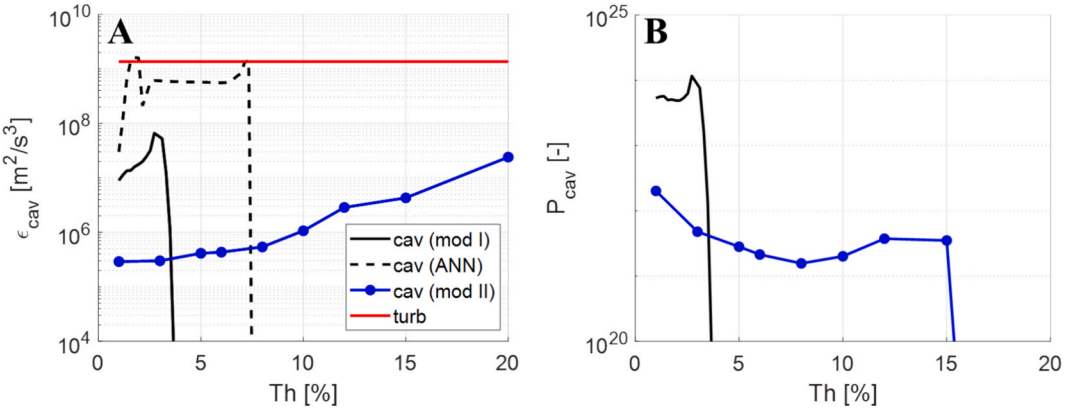

Fig. 9. A) Cavitation intensity (black and blue), compared to the dissipation rate of TKE in the HPH jet (red), as a function of the Thoma number, Th. B) Cavitation performance (Eq. (11)) as a function of the Thoma number, Th. For cavitation, the figure compares results from using a simplistic pressure profile (model I, black solid line), based on the CFD-DPM pressure profiles (model II, blue markers), and a previously suggested ANN model (Ranade and Ranade, 2023) (dashed black line). (Δp = 26 MPa).

increases with *Th* since increasing *Th* lifts the pressure further above the vapour pressure (see Fig. 8A).

The dashed line in Fig. 9A displays the estimations from the ANN (Ranade and Rande, 2023). Here, the ANN deviates more from the simulations than in Fig. 7. However, note that it does predict both a local maximum and a sharp decrease when the Thoma number approaches a critical value.

The blue markers in Fig. 9A display ε_{cav} estimated from using the pressure on the CFD trajectories in determining the time-average pressure in Eq. (7) (i.e., model II). As with the simplified model (model I), ε_{cav} increases with *Th*. However, there is no longer a sharp limit below which no implosions take place.

Some further insights into the difference between the two modelling approaches can be obtained from Fig. 10 showing contours of the reduced pressure ratio, $(p\text{-}p_{vap})/p_2$, for three Thoma numbers (at Δp = 26 MPa) with an overlay of example trajectories (the view displays only ~10 tracks per case in order not to clutter the view). Note that Thoma number has two different effects. First, operating at a low Thoma number creates large variations in static pressure along trajectories, partly since the region where the static pressure reaches close to the vapour pressure is larger, but also because it allows for a static pressure that is–locally–substantially higher than the backpressure. The global maximum of the reduced pressure ratio reaches up to ~20 for Th = 1 % (as compared to ~5 for Th = 5 % and ~2 for Th = 20 %). (Note, however, that the colour scale in Fig. 10 has been capped at $(p\text{-}p_{vap})/p_2$ = 2.0, to more clearly show difference across the whole domain.) Secondly, also note that the Thoma number influences the vapour bubble trajectories. This is due to changes in the location of the HPH outlet chamber jet. The HPH outlet chamber jet without cavitation (or with limited cavitation) attaches to the forcer incline (Innings and Trägårdh, 2007; Håkansson et al., 2011; Håkansson, 2024). Extensive cavitation lifts the jet from the forcer wall (Rütten and Håkansson, 2025). This also changes the trajectories of the vapour bubbles.

The dissipation rate of TKE has also been included in Fig. 9A (red line, Eq. (22)). If the ANN is disregarded (since it is not trained on conditions similar to the HPH, it is of less relevance for making quantitative comparisons), the results from Section 3.3 hold; substantially more energy is dissipated due to turbulence than from cavitation implosions in the HPH. This applies regardless of the value of *Th*.

Fig. 9B displays the cavitation performance as a function of Thoma number. Again, the quantitative values differ depending on if model I or model II is used for describing the time-averaged external static pressure. However, both methods suggest P_{cav} to increase to a local maximum and then rapidly decrease to zero beyond a critical value. It is interesting to note that using the CFD-trajectory method (model II), this critical *Th* beyond which no cavitation implosions are expected, is substantially higher than what is obtained with model I (or the Blake threshold analysis, which was also based on model I, see Section 3.2). With method II, the threshold is calculated to be Th = 12 %, which is more in line with experimental findings (Håkansson et al., 2010; Kurzhals, 1977; Lander et al., 2000).

3.5. Formation of free radicals

Several authors have used versions of the so-called Weissler reaction (Weissler et al., 1950) to measure cavitation intensity in HPHs (Floury et al., 2004; Lander et al., 2000; Shirgaonkar et al., 1998). The method measures the free radicals formed due to cavitation implosions. These studies typically find an increase in free radical formation with homogenizing pressure and a decrease with increasing Thoma number (Floury et al., 2004; Lander et al., 2000; Shirgaonkar et al., 1998).

As discussed in Section 2.8, the hot-spot theory suggests that free radical formation is driven by the high implosion temperatures and high pressures inside of the vapour bubble at collapse, in combination with the chemical composition. Fig. 11 displays the maximum temperature, $T_{B,\max}$, and pressure, $p_{B,\max}$, as functions of homogenizing pressure and Thoma number. The maximum bubble temperature has a relatively weak dependence on homogenizing pressure (Fig. 11A) and a small increase with Δp above 20 MPa. More noticeably, $T_{B,\max}$, decreases rapidly down to ~300 K if increasing the Thoma number above ~3.5 % (as expected from how this prevents any catastrophic implosion, see Section 3.2). The maximum implosion pressure decreases somewhat with increasing homogenizing pressure (Fig. 11C). Moreover, the suppression of implosion when applying a backpressure is also evident from $p_{B,\max}$ (Fig. 11D).

Fig. 12A and B display the resulting mole fraction of the hydroxyl radical as a function of homogenizing pressure (Fig. 12A) and Thoma number (Fig. 12B). The concentration of hydroxyl radicals decreases slightly with increasing homogenizing pressure and increases rapidly with increasing Thoma number.

However, the mole fraction describes what is generated in a single bubble collapse. The hydroxyl radical performance, $P_{\bullet OH}$ (mole fraction multiplied with number of vapour bubbles, see Eq. (20), can be seen in Fig. 12C and D. As seen in Fig. 12C, the free radical performance of the HPH valve increases with homogenizing pressure until leveling off at approximately 25–30 MPa (i.e., at a relatively high homogenizing pressure for this valve design). Moreover, the free radical performance is predicted to decrease with Thoma number, until being supressed at a sufficiently high *Th*. Note that since the analysis in this section is based on the external pressure profile from model I, this critical Thoma

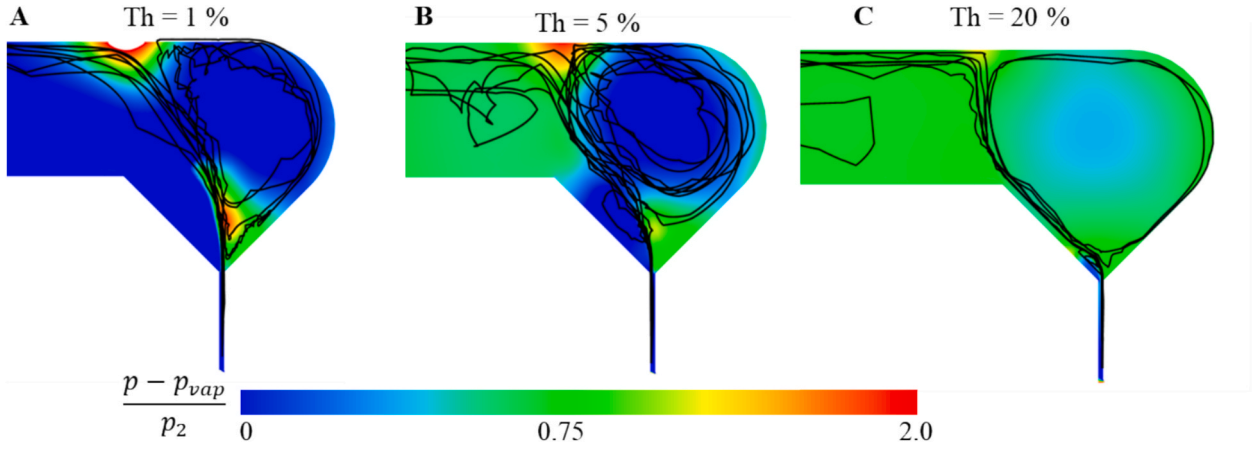

Fig. 10. Contours of reduced pressure, $(p\text{-}p_{vap})/p_2$, of a HPH valve operating at Δp = 26 MPa at three different Thoma numbers (Th = 1 %, 5 % and 20 %), overlayed with examples of particle trajectories. (Figure only shows the gap and outlet chamber; the reduced pressure is substantially higher in the inlet chamber, and thus, no cavitation takes place here, see Rütten and Håkansson (2025).

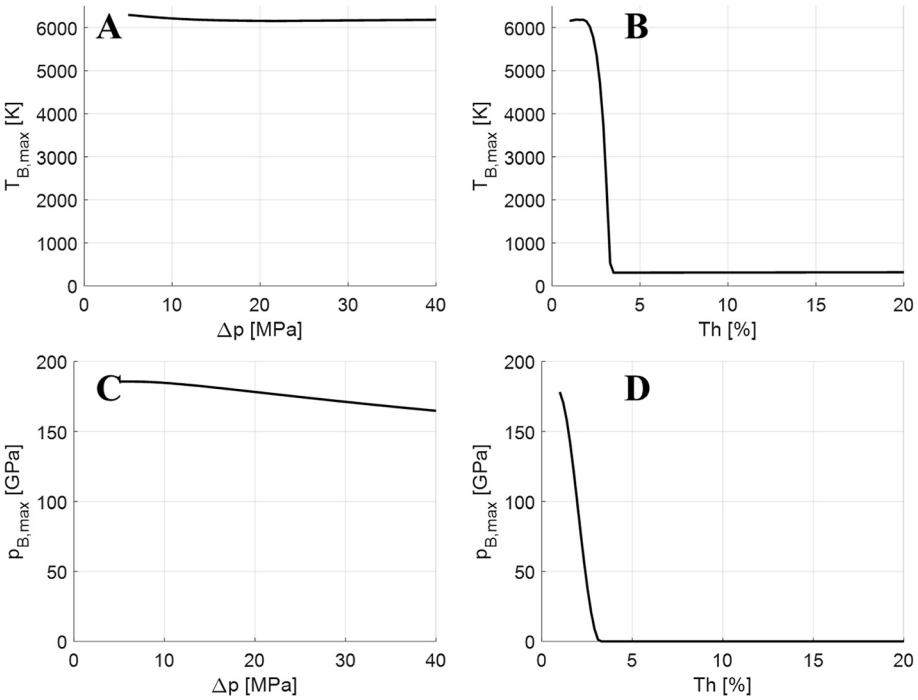

Fig. 11. Maximum bubble temperature, T_B (A-B), and bubble pressure, p_B (C-D), as a function of (A, C) homogenizing pressure, Δp (at Th = 1 %), or (B, D) Thoma number, Th (at Δp = 20 MPa).

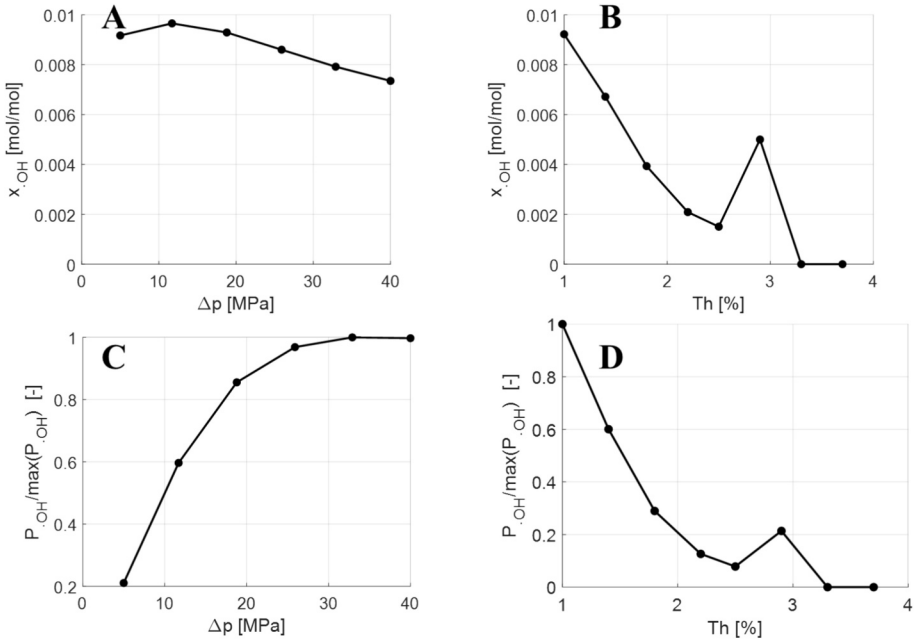

Fig. 12. Predicted formation of free radicals as a function of operating conditions. A-B) Mole fraction of the hydroxyl radical, $x_{\bullet OH}$, as a function of (A) homogenizing pressure, Δp (at Th = 1 %), and (B) as a function of Thoma number (at Δp = 20 MPa). Hydroxyl radical load, $L_{\bullet OH}$, as a function of (A) homogenizing pressure, Δp (at Th = 1 %), and (B) as a function of Thoma number (at Δp = 20 MPa).

number is very low. It should also be noted that the increase in hydroxyl radical creation with homogenizing pressure and the suppression when applying a backpressure is (qualitatively) in agreement with experimental findings discussed by, for example, Floury et al. (2004) and Shirgaonkar et al. (1998). Another observation is that the local maxima become less pronounced when considering the number of vapour bubbles (similarly to what was seen in Section 3.4).

Here it should be noted that some concerns have been raised against using free radical formation as a measure of cavitation intensity in hydrodynamic cavitation (Morisson and Hutchinson, 2009), due to spurious results which could be due to consumption reaction(s) (Gutierrez et al., 1991). Note that these effects are not included in Fig. 12, which presents the predictions based on the assumption that the mole fraction of the hydroxyl radical seen exiting the HPH is directly proportional to that formed in equilibrium at the most violent vapour bubble collapse.

3.6. Towards predictive modelling of HPH valve cavitation

The long-term objective of our endeavours is to allow for model-based design to optimize HPH operation and valve design. This requires a set of models that can predict inception, extent and intensity of cavitation as a function of operating parameters, fluid properties, and valve geometry. In the light of the current study, it is interesting to discuss to what extent this has been achieved and what remains for future studies.

From the discussion above, we argue that the modelling framework captures realistic trends compared to what has been observed in experimental studies. For example, the CFD model connected to a macroscopic cavitation model (Rütten and Håkansson, 2025) predicts that cavitation inception is, mainly, controlled by Thoma number. Moreover, the model predicts that the Thoma number shifts the region where cavitation-induced microjets occur in a manner that is consistent with experimental studies on wear.

The modelling framework also predicts an increase in cavitation intensity with homogenizing pressure and a decrease with Thoma number (Sections 3.3-4). This agrees with a number of previously reported experimental studies. Moreover, the model can also reproduce the previously reported trends in free radical formation with homogenizing pressure and Thoma number (Section 3.5), at least qualitatively. The finding that the cavitation-induced kinetic energy dissipation rate is substantially lower than the dissipation rate of TKE also helps explain previous experimental studies showing that cavitation does not aid in emulsion drop breakup in HPHs (Gothsch et al., 2016; Preiss et al., 2022; Schlender et al., 2015). Moreover, the finding that extensive cavitation shifts the macroscopic jet, making it detach from the forcer wall, can help explain why these experimental studies see a decreasing breakup efficiency in the presence of extensive cavitation in HPHs.

However, before concluding that the proposed modelling framework can be applied in a model-based design workflow, further experimental validation is desired. As noted above, assumptions are employed and fitting constants are used in deriving the modelling framework, for example in employing the hot-spot theory for free radical formation (Section 2.8), in the choice of the initial gas bubble radius (Section 2.5), and in the modelling of external pressure fluctuations (Section 2.4).

Unfortunately, it is not straight-forward to design such experiments. Although several methods have been proposed for quantifying cavitation, it is difficult to link the methods directly to cavitation intensity in the HPH. For example, for the abovementioned free-radical based method, experiments suggest that there are simultaneously occurring consumption reactions, alternatively free radical formation is too low to give rise to a sufficiently high signal-to-noise ratio (Beekwilder and Sevrell, 2025; Morisson and Hutchinson, 2009). For ultrasonics-based methods, there have been reports that extensive cavitation attenuates the implosion sound waves and, thus, the measured ultrasonic amplitude might not be a good indication of cavitation above a certain critical extent of cavitation (Franc and Michel, 2005; Håkansson et al., 2010). Continued development of experimental strategies to validate the modelling framework suggested here will be an interesting continuation of the present contribution.

4. Conclusions

This contribution applies a method for modelling cavitation intensity in HPH to understand some apparent contradictions in the literature on cavitation in HPHs. In summary:

- Whereas the extent of cavitation (e.g., volume fraction of vapour accumulated in the valve) decreases with homogenizing pressure (if keeping *Th* constant), the cavitation intensity (i.e., the rate of energy dissipation due to microjet implosion following bubble implosion) increases with homogenizing pressure. Since it is cavitation bubble implosions that drive wear, ultrasonic emissions, droplet breakage and free radical formation, this helps explain why experimental investigations typically find an increase in cavitation signal with homogenizing pressure.
- Cavitation number has often been used to describe both extent and intensity of cavitation in HPHs. However, the results above indicate that, whereas cavitation number is a suitable measure of cavitation inception and extent (Rütten and Håkansson, 2025), it cannot (alone) describe cavitation intensity.
- For the HPH, the dissipation rate of energy due to bubble implosion is orders of magnitude lower than the dissipation rate of turbulent kinetic energy in a HPH, even if the HPH is operated to give extensive cavitation. This contrasts with devices operating at much lower pressures (compared to HPH) where cavitation is seen to control breakup. This helps to explain why extensive cavitation in HPH has not been seen to aid in drop breakup in previous experimental studies.
- When the HPH is operated with a backpressure, this not only reduces the extent of cavitation (i.e., number of cavity implosions), but also influences the intensity of each cavity collapse (i.e., it influences cavitation intensity). Results suggest that the cavitation intensity initially increases with increasing backpressure. However, when a critical level is reached, the pressure fluctuations become too low in comparison to the backpressure, thus, preventing any implosions altogether.
- Combined with a hot-spot theory approach, the methodology can also be used to predict free radical formation, and the observed trends are (qualitatively) consistent with those seen in previously published experimental studies.

The presented approach and framework will be useful for practicing engineers and researchers interested in developing predictive models for simulating performance of HPH for variety of applications.

CRediT authorship contribution statement

Andreas Håkansson: Writing – original draft, Supervision, Investigation, Conceptualization. **Eva Rütten:** Writing – review & editing, Visualization, Methodology. **Vivek V. Ranade:** Writing – review & editing, Methodology, Conceptualization.

Declaration of competing interest

The authors declare that they have no known competing financial interests or personal relationships that could have appeared to influence the work reported in this paper.

Acknowledgments

AH acknowledges founding from the Swedish Research Counsil (VR), grant number 2024-04823.

Appendix A. Supplementary data

Supplementary data to this article can be found online at https://doi.org/10.1016/j.ces.2025.121896.

Data availability

Data will be made available on request.

References

Bale, C.W., Bélisle, E., Chartrand, P., Decterov, S.A., Erkisson, G., et al., 2009. FactSage thermochemical software and databases — recent developments. Graphad 33, 295–311. https://doi.org/10.1016/j.calphad.2008.09.009.

Beekwilder, P., Sevrell, F., 2025. Cavitation in High-Pressure Homogenizers–Investigation of an Experimental Method Based on Free Radical

Formation. MSc thesis, Department of Process and Life Science Engineering, Lund University, Lund, Sweden.
Carpenter, J., Pinjari, D.V., Saharan, V.K., Pandit, A.B., 2022. Critical review on hydrodynamic cavitation as an intensifying homogenizing technique for oil-in-water emulsification: theoretical insight, current status, and future perspectives. Ind. Eng. Chem. Res. 61, 10587–10602. https://doi.org/10.1021/acs.iecr.2c00754.
Chakma, S., Moholkar, V.S., 2013. Numerical simulation and investigation of system parameters of sonochemical process. Chin. J. Eng. 2013, 362682. https://doi.org/10.1155/2013/362682.
Chaudhuri, J.H., Chatterjee, D., 2024. Modelling of chemical kinetics in the presence of hydrodynamic cavitation for wastewater treatment applications. Chem. Eng. Sci. 295, 120167. https://doi.org/10.1016/j.ces.2024.120167.
Dastane, G.G., Thakkar, H., Shah, R., Perala, S., Raut, J., Pandit, A.B., 2019. Single and multiphase CFD simulations for designing cavitating venturi. Chem. Eng. Res. Des. 149, 1–12. https://doi.org/10.1016/j.cherd.2019.06.036.
Ding, W., Hong, F., Ying, D., Huang, Y., Khan, S.N., Jia, J., 2024. A comprehensive study on the effects of annular protrusion for cavitation intensification in Venturi tubes. Chem. Eng. J. 498, 155306. https://doi.org/10.1016/j.cej.2024.155306.
Floury, J., Legrand, J., Desrumaux, A., 2004. Analysis of a new type of high pressure homogeniser. Part B. Study of droplet break-up and recoalescence phenomena. Chem. Eng. Sci. 59, 1285–1294. https://doi.org/10.1016/j.ces.2003.11.025.
Franc, J.-P., Michel, J.-M., 2005. Fundamentals of Cavitation. Springer Science, Berlin.
Gao, G., Guo, S., Li, D., 2024. A review of cavitation erosion on pumps and valves in nuclear power plants. Materials 17, 1007. https://doi.org/10.3390/ma17051007.
Gode, A., Madane, K., Ranade, V.V., 2023. Design of vortex-based cavitation devices/reactors: influence of aspect ratio, number of inlets and shape. Ultrason. Sonochem. 101, 106696. https://doi.org/10.1016/j.ultsonch.2023.106695.
Gogate, P.R., Shirgaonkar, I.Z., Sentihilkumar, P., Vichare, N.P., Pandit, A.B., 2001. Cavitation reactors: efficiency assessment using a model reaction. AIChE J. 47, 2526–2538. https://doi.org/10.1002/aic.690471115.
Gothsch, T., Schilcher, C., Richter, C., Beinert, S., Dietzel, A., Büttgenbach, S., Kwade, A., 2015. High-pressure microfluidic systems (HPMS): flow and cavitation measurements in supported silicon microsystems. Microfluid. Nanofluid. 18, 121–130. https://doi.org/10.1007/s10404-014-1419-6.
Gothsch, T., Richter, C., Beinert, S., Schilcher, C., Schilde, C., Büttgenbach, S., Kwade, A., 2016. Effect of cavitation on dispersion and emulsification process in high-pressure microsystems (HPMS). Chem. Eng. Sci. 144, 239–248. https://doi.org/10.1016/j.ces.2016.01.034.
Gogate, P.R., Pandit, A.B., 2000. Engineering design methods for cavitation reactors II: hydrodynamic cavitation. AIChE J 46, 1641–1649. https://doi.org/10.1002/aic.690460815.
Gutierrez, M., Henglein, A., Ibanez, F., 1991. Radical scavenging in the sonolysis of aqueous solutions of iodide, bromide and azide. J. Phys. Chem. 95, 6044. https://doi.org/10.1021/j100168a061.
Håkansson, A., Fuchs, L., Innings, F., Revstedt, J., Bergenståhl, B., Trägårdh, C., 2010. Visual observations and acoustic measurements of cavitation in an experimental model of a high-pressure homogenizer. J. Food Eng. 100, 504–513. https://doi.org/10.1016/j.jfoodeng.2010.04.038.
Håkansson, A., Fuchs, L., Innings, F., Revstedt, J., Trägårdh, C., Bergenståhl, B., 2011. High resolution experimental measurement of turbulent flow field in a high pressure homogenizer model its implication on turbulent drop fragmentation. Chem. Eng. Sci. 66, 1790–1801. https://doi.org/10.1016/j.ces.2011.01.026.
Håkansson, A., 2019. Emulsion formation by homogenization: current understanding and future perspectives. Annu. Rev. Food Sci. Technol. 10, 239–258. https://doi.org/10.1146/annurev-food-032818-121501.
Håkansson, A., 2024. High-pressure homogenizer valve design modifications allowing intensified drop breakup without increasing power consumption. I. Optimization of current design-principle. Chem. Eng. Process.–Proc. Intensif. 196. https://doi.org/10.1016/j.cep.2023.109659.
Håkansson, A., 2025. A low-cost method for characterizing the inception and extent of cavitation in high-pressure homogenizers. Ind. Eng. Chem. Res. 64 (15), 7893–7902. https://doi.org/10.1021/acs.iecr.5c00512.
Harkin, A., Nadim, A., Kaper, T.J., 1999. On acoustic cavitation of slightly subcritical bubbles. Phys. Fluids 11, 274–287. https://doi.org/10.1063/1.869878.
Hong, F., Xue, H., Yuan, X., Wang, L., Tian, H., Ye, L., Jia, J., Ying, D., Huang, Y., 2023. Numerical investigation on the hydrodynamic performance with special emphasis on the cavitation intensity detection in a Venturi cavitator. Process Saf. Environ. Prot. 175, 212–226. https://doi.org/10.1016/j.psep.2023.05.037.
Innings, F., Trägårdh, C., 2007. Analysis of the flow field in a high-pressure homogenizer. Exp. Therm Fluid Sci. 32, 345–354. https://doi.org/10.1016/j.expthermflusci.2007.04.007.
Innings, F., Hultman, E., Forsberg, F., Prakash, B., 2011. Understanding and analysis of wear in homogenizers for processing liquid food. Wear 271, 2588–2598. https://doi.org/10.1016/j.wear.2011.01.084.
Kalmár, C., Turányi, T., Zsély, I.G., Papp, M., Hegedüs, F., 2022. The importance of chemical mechanisms in sonochemical modelling. Ultrason. Sonochem. 83, 105925. https://doi.org/10.1016/j.ultsonch.2022.105925.
Keller, J.B., Miksis, M., 1980. Bubble oscillations of large amplitude. J. Acoust. Soc. Am. 68 (2), 628–633. https://doi.org/10.1121/1.384720.
Kumar, P., Khanna, S., Moholkar, V.S., 2012. Flow regime maps and optimization thereby hydrodynamic cavitation reactors. AIChE J 58, 3858–3866. https://doi.org/10.1002/aic.13771.
Kurzhals, H.-A., 1977. Untersuchungen über die physikalisch-technischen Vorgänge beim Homogenisieren von Milch in Hochdruck-Homogenisiermaschinen. Doctoral Thesis, University of Hannover.
Lander, R., Manger, W., Scouloudis, M., Ku, A., Davis, C., Lee, A., 2000. Gaulin homogenization: a mechanistic study. Biotechnol. Prog. 16, 80–85. https://doi.org/10.1021/bp990135c.
Li, D., Xi, Y., Li, R., Hong, F., Yuan, X., Huang, D., Johnson, D., Lv, Y., Huang, Y., 2025. Investigation on the mechanism of Cr(VI) reduction driven by hydrodynamic cavitation: comprehensive analysis of the bubble dynamics and free radical generation. Sep. Purif. Technol. 368, 133058. https://doi.org/10.1016/j.seppur.2025.133058.
Li, L., Pei, C., Wang, Z., Lin, Z., Li, X., Zhu, Z., 2024. Assessment of cavitation erosion risk by Eulerian–Lagrangian multiscale modelling. Int. J. Mech. Sci. 262, 108735. https://doi.org/10.1016/j.ijmecsci.2023.108735.
Maleki, M., Talabazar, F.R., Davoudian, S.H., Dular, M., Kosar, A., Petrovsek, M., Smid, A., Zupanc, M., Ghorbani, M., 2025. The formation of hydroxyl radicals during hydrodynamic cavitation in microfluidic reactors using salicylic acid dosimetry. Chem. Eng. J. 511, 161976. https://doi.org/10.1016/j.cej.2025.161976.
Moholkar, V.S., 2001. Modeling of hydrodynamic cavitation reactors: a unified approach. Chem. Eng. Sci. 56, 6295–6302. https://doi.org/10.1016/S0009-2509(01)00253-6.
Moholkar, V.S., Pandit, A.B., 1997. Bubble behavior in hydrodynamic cavitation: effect of turbulence. AIChE J 43, 1641–1648. https://doi.org/10.1002/aic.690430628.
Morisson, K.R., Hutchinson, C.A., 2009. Limitations of the Weissler reaction as a model reaction for measuring the efficiency of hydrodynamic cavitation. Ultrason. Sonochem. 16, 176–183. https://doi.org/10.1016/j.ultsonch.2008.07.001.
Olad, P., Crialesi-Esposito, M., Brandt, L., Innings, F., Håkansson, A., 2022a. A DNS investigation of the one-phase flow in a simplified emulsification device. J. Fluids Eng. 144, 081209. https://doi.org/10.1115/1.4053896.
Olad, P., Crialesi, M., Brandt, L., Innings, F., Håkansson, A., 2022b. Towards best practice recommendations for turbulence modelling of high-pressure homogenizer outlet chambers – Numerical validation using DNS data. Chem. Eng. Sci. 258, 117748. https://doi.org/10.1016/j.ces.2022.117748.
Pandit, A.V., Sarvothaman, V.P., Ranade, V.V., 2021. Estimation of chemical and physical effects of cavitation by analysis of cavitating single bubble dynamics. Ultrason. Sonochem. 77, 105677. https://doi.org/10.1016/j.ultsonch.2021.105677.
Pawar, S.K., Mahulkar, A.V., Pandit, A.B., Roy, K., Moholkar, V.S., 2017. Sonochemical effect induced by hydrodynamic cavitation: comparison of venturi/orifice flow geometries. AIChE J. 63, 4705–4716. https://doi.org/10.1002/aic.15812.
Perdih, T.S., Zupanc, M., Dular, M., 2010. Revision of the mechanisms behind oil-water (O/W) emulsion preparation by ultrasound and cavitation. Ultrason. – Sonochem. 51, 298–304. https://doi.org/10.1016/j.ultsonch.2018.10.003.
Pope, S.B., 2000. Turbulent Flows. Cambridge University Press, Cambridge, UK.
Preiss, F.J., Hetz, M., Karbstein, H.P., 2021. Does cavitation affect droplet breakup in high-pressure homogenization? Insights into local effect. Chem. Ing. Tech. 94, 374–384. https://doi.org/10.5445/IR/1000136030.
Ranade, N.V., Ranade, V.V., 2023. ANN based surrogate model for key Physico-chemical effects of cavitation. Ultrason. Sonochem. 94, 106327. https://doi.org/10.1016/j.ultsonch.2023.106327.
Rütten, E., Håkansson, A., 2025. A CFD-based Approach to Study Cavitation in High-pressure Homogenizer Valves. Part 1. Cavitation inception, extent and location. Part 1 of this series, submitted simultaneously.
Sauer, T., 2012. Numerical Analysis. Pearson. p. 250. ISBN 978-0-321-78367-7.
Sawant, S.S., Anil, A.C., Krishnamurhy, V., Gaonkar, C., Kolwalkar, J., et al., 2008. Effect of hydrodynamic cavitation on zooplankton: a tool for disinfection. Biochem. Eng. J. 42, 320–328. https://doi.org/10.1016/j.bej.2008.08.001.
Schlender, M., Spengler, A., Schuchmann, H.P., 2015. High-pressure emulsion formation in cylindrical coaxial orifices: influence of cavitation induced pattern on oil drop size. Int. J. Multiph. Flow 74, 84–95. https://doi.org/10.1016/j.ijmultiphaseflow.2015.04.004.
Schlender, M., Minke, K., Schuchmann, H.P., 2016. Sono-chemiluminescence (SCL) in a high-pressure double stage homogenization processes. Chem. Eng. Sci. 142, 1–11. https://doi.org/10.1016/j.ces.2015.11.028.
Shirgaonkar, I.Z., Lothe, R.R., Pandit, A.B., 1998. Comments on the mechanism of microbial cell disruption in high-pressure and high-speed devices. Biotechnol. Progr. 14 (4), 657–660. https://doi.org/10.1021/bp980052g.
Simpson, A., Renade, V.V., 2018. Modeling of hydrodynamic cavitation with orifices: influence of different orifice designs. Chem. Eng. Res. Des. 136, 698–711. https://doi.org/10.1016/j.cherd.2018.06.014.
Simpson, A., Renade, V.V., 2019. Flow characteristics of a vortex based cavitation device. AIChE J. 65, e16675. https://doi.org/10.1002/aic.16675.
Sreedhar, B.K., Albert, S.K., Pandit, A.B., 2017. Cavitation damage: theory and measurements – a review. Wear 372–373, 177–196. https://doi.org/10.1016/j.wear.2016.12.009.
Thaker, A.H., Ranade, V.V., 2023. Drop breakage in a single-pass through vortex-based cavitation device: experiments and modeling. AIChE J 69 (1), e17512. https://doi.org/10.1002/aic.17512.
Thaker, A.H., Ranade, V.V., 2022. Towards harnessing hydrodynamic cavitation for producing emulsions: breakage of an oil drop in a vortex based cavitation device. Chem. Eng. Process. - Process Intesif. 180, 108753. https://doi.org/10.1016/j.cep.2021.108753.
Weissler, A., Cooper, H.W., Snyder, S., 1950. Chemical effect of ultrasonic waves: oxidation of potassium iodide solution by carbon tetrachloride. J. Am. Chem. Soc. 72 (4), 1769–1775. https://doi.org/10.1021/ja01160a102.
Wu, P., Bai, L., Lin, W., 2020. On the definition of cavitation intensity. Ultrasonics –. Sonochemistry 67, 105141. https://doi.org/10.1016/j.ultsonch.2020.105141.
Yang, Q., Chen, M., Pei, C., Liu, B., Zhao, M., Wang, X., Lin, Z., Li, L., 2025. Experimental and Eulerian-Lagrangian numerical investigation on cavitation erosion

characteristics in Venturi pipes with different divergent angles. Ultrasonic Sonochemistry 114, 107278. https://doi.org/10.1016/j.ultsonch.2025.107278.